Raman analyses and "smart" imaging of nanophases and nanosized materials

Philippe Colomban

LADIR-UMR 7075 CNRS & Université P. & M. Curie, 2 rue Henry Dunant, 94320 Thiais, France

Technological advances have increased significantly the performance of Raman instruments over the past decade. On-site measurements are now relatively easy, and controlled mapping of materials and devices allows consecutive spectra to be recorded stepwise with a lateral spatial resolution close to 0.5 μm. 100 × 100 point maps can be recorded on a reasonable timescale with high sensitivity Raman instruments. The Raman spectral parameters in these maps can be used to generate "smart" images showing, for example, compositional, structural, short-range order or particle size variation and information. This is important to the study of nanostructured/nanocrystalline materials, since most of their mechanical/electrical properties are controlled by particle size. Raman spectra and their "smart" images can be used to understand and even predict some properties. In addition, in some cases (for example a coloured phase dispersed in a translucent matrix), the elastic (Rayleigh) scattering, which is orders of magnitude higher than the inelastic Raman scattering, can be used to obtain quasi-instantaneous images of a material's skin, which is important, for example in corrosion studies, for observing surface composition or roughness change. Rayleigh imaging can offer very similar information as AFM for second phase carbon-containing materials.

Nanomaterials and nanotechnology

Reducing the dimension of matter domains down to the nanometre scale produces entities exhibiting unique properties. These so-called nanomaterials (i.e. materials with one dimension <50–100 nm) have been made since the first traditional ceramics appeared. For instance, the plasticity, shapeability, rheology, slip formation, low sintering temperature etc. of pottery are directly related to the fact that natural clay is a nanosized layer (slab) and the "so-called" sol–gel route only results from the transposition of the clay route to simpler, e.g. oxide, carbide, compositions.[1,2] In the last ten centuries, nanosized ceramic pigment powders have also been created to colour enamels and glass. Because of the sharpness of the human eye, a pigment must have a particle size close to 500 nm or less to give the appearance of homogeneous colouration. Moreover, polychrome Abbasid lustre potteries (9th century) consist of a nano-grating made of Ag and Cu metal particles regularly embedded in the glaze.[3]

Market forces and ecology considerations that include a desire to use our limited resources more efficiently for a sustainable development drive efforts at miniaturisation. A great variety of nanomaterials are now being developed, if not already commercially available, for applications taking advantage of their: (i) optical properties (e.g. pigments in traditional ceramics and for the cosmetics industry, fluorescent markers, quantum dots, photonic crystals for multiplexing and switching in optical networks, quantum computer components); (ii) mechanical properties (e.g. fibres, wear-resistant and anti-corrosion films, cutting coatings, "nano-polishing" SiC-, diamond-, boron carbide-powders, high impact strength nanocomposites); (iii) magnetic properties (e.g. data storage, reading heads, GMR (Giant Magneto-Resistive) materials); (iv) high specific surface area (e.g. propulsion, filters, nanosensors, semiconductor nanowires, catalysts); (v) electrical properties (e.g. miniaturised silicon chips, single electron transistors, carbon nanotubes or even silicon nanotubes transistors) and (vi) biocompatibility (e.g. *in vivo* drug delivery, diagnostic and monitoring devices).

The challenge for the "so-called" nanotechnologies is to achieve perfect control on nanoscale-related properties. Advanced devices are made of various materials with additional films, coatings etc. Imaging the different materials, their composition, structure and other characteristics is essential in order to optimise their processing, their properties and the cost of the final device. This clearly requires correlating the parameters of the synthesis process with the resulting nanostructure. Not all conventional techniques are suited for characterising the nanostructure [or, like Transmission Electronic Microscopy (TEM), require complex sample preparation]. In the last few years, technological advances have made relatively inexpensive Raman instruments available. Modern Raman spectrometers offer the great advantages of non-destructive analysis and some are readily transportable, enabling their use for on-site analysis. In addition to providing basic phase identification, Raman spectra through subtle variations may be used also to assess some properties that are characteristic of the nanoscale. Moreover, the technique also allows for imaging of the materials and their properties.

The Raman effect in nanomaterials

Raman spectroscopy has an intrinsic "nano-specificity" since it probes the iono-covalent bonds of materials. The sample volume probed by Raman microscopy is very small, typically *ca.* 1–5 μm^3, so even in extended domains, it is nano-domains that are being studied. Vibrational stretching modes are highly characteristic of the chemical bond and allow for composition identification. Bending vibrational modes are more sensitive to the neighbouring

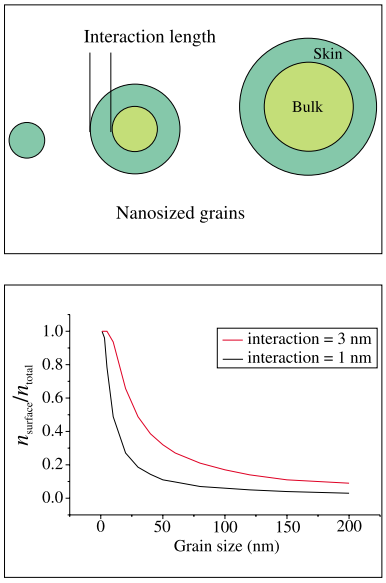

Figure 1. Top, schematic representation of the relative proportion of bulk and skin matter volumes for nanosized grains. Bottom, the proportion of atoms in the skin and in the bulk has been calculated for two interaction lengths representative of covalent (1 nm) and ionic (3 nm) material, respectively.

entities and, hence, to short-range order. Librational and external modes, which depend on the structure, correspond to relative motions of whole units of a molecule. Well-defined repetitive structures (e.g. crystalline domains) will typically give rise to Raman spectra with sharp well-resolved peaks, whereas spectra with broad bands indicate that different configurations and/or many electric or mass defects exist in the material. Thus if the proportion of atoms belonging to the (near-) surface region contributing to the Raman spectrum is significant, the disorder related to the various atomic arrangements will contribute significantly to the observed Raman features.[4] We can say empirically that the chemical bonds located as far as 5–15 atomic distances from the skin atoms have a state different from those in the bulk (Figure 1). Considering that a bond length is close to 0.15–0.2 nm (5/6 atoms per nm) and assuming a cubic shape, a grain with a side dimension of 1 nm consists of a cube with $6 \times 6 \times 6 = 216$ atoms. All atoms will then appear to be "surface-like", no matter what interaction length we chose (either five atomic distances = 1 nm or 15 atomic distances = 3 nm). For a grain of 3 nm size and a 1 nm interaction length, the bulk consists of a cube of 1 nm sides. Assuming a cubic shape for the grains, the number of atoms perturbed by the surface vs the total number is given in Figure 1 for interaction lengths of 1 and 3 nm. It is obvious that vibrational properties of surface atoms will dominate the spectra for a grain size <20 nm (1 nm interaction length) or <50 nm (3 nm interaction length). Assuming a spherical shape for the grains, the perturbation would decrease more rapidly. When the surface atoms contribute significantly to the Raman scattering (we arbitrarily chose a 15% limit in Figure 1), the effects of periodicity no longer dominate and all vibrational modes, in particular those located away from the Brillouin zone (BZ) centre ($q = 0$) contribute significantly to the spectra. We observe a so-called "density-of-state" projection, like in amorphous compounds (Figure 2).[5–7] The unidirectional (1D) stacking disorder observed in SiC compounds is a good example of the different losses of periodicity possible, from a step by step increasing of the unit-cell parameter along the stacking axis (formation of specific polytypes: 2H, 3H, 6H, …) to a density-of-state projection when the stacking of the basic SiC structure becomes fully disordered. SiC structures alternate layers of Si and C atoms. Two consecutive layers form a bilayer that is named "H" if the layers are identical and merely separated by a translation. If not, when an additional 180° rotation (around the Si–C bond linking the bilayers) is necessary to get the superposition, then the bilayer is named "K". The "K" only stacking is found in the reference material β-SiC with cubic symmetry (3C or β phase), which has main Raman peaks centred at 797 and 972 cm^{-1} corresponding to the transverse optic (TO) and longitudinal optic (LO) modes, respectively. Any other definite stacking sequence is called α-SiC (the collection of all polytypes) and has either hexagonal or rhombohedral lattice symmetry.[8]

Correlation between Raman parameters and grain size

Many techniques for the preparation of nanosized materials [e.g. sol–gel, thermal treatment of polymeric precursor, electrochemical deposition, atomic layer deposition (ALD) etc.] lead to amorphous or low crystallinity compounds by quenching of a liquid-state local structure or a very disordered state. Two phenomena can be at the origin of the broadening of the Raman spectrum: (i) the loss of periodicity because of the large contribution to the

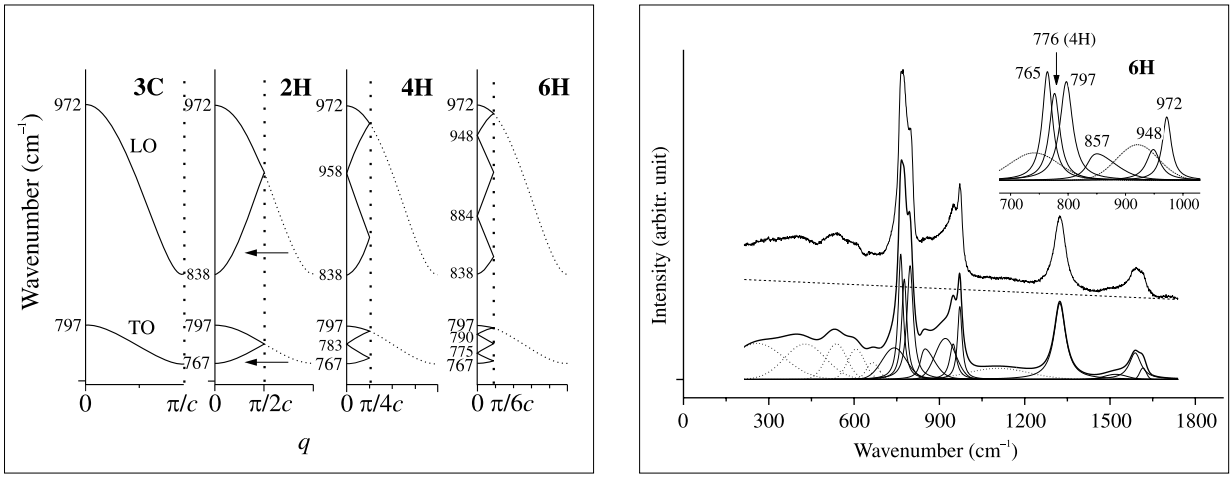

Figure 2. Left, schematic of the Brillouin zone (BZ) folding when the unit cell *c* parameter of SiC phase increases by ×2, ×3, ×4; the reciprocal BZ reduces accordingly. Right, an example of a Raman spectrum of a SiC fibre containing several SiC polytypes (+ carbon 2nd phase).

molecular vibrations of surface atoms, (ii) a low crystallinity, that is to say short-range disorder or bond distortion. In many cases the exact origin is not obvious and complementary information must be obtained using transmission electronic microscopy.[9]

Different models have been used to derive the particle size from Raman spectra: Duval's model (DM) relies on the position of acoustic peaks,[10] whereas the phonon confinement model (PCM) fits the asymmetry associated with Raman peaks of nanoparticles as a function of the grain size.[5,7,11] Specific models for carbon grains, based on the relative intensity of the D-band, *ca.* 1355 cm^{-1}, ("surface" layer of nano-sized carbon particles with hybridisation intermediate between sp^2 and sp^3) and the G-band, *ca.* 1590 cm^{-1}, (bulk of graphite nanocrystallites with sp^2 hybridisation) have been developed.[12,13]

As an example, we shall briefly explain the PCM. The scattering of one photon by *n* phonons is governed by the momentum conservation. Only vibrations from the centre of the Brillouin zone (CBZ) should therefore be active in a one-phonon process (first order Raman spectrum) and this is actually the case in large and flawless crystals, where phonons virtually propagate to "infinity". However, short-range disorder, bond distortion or nano-crystallinity, can destroy periodicity and confine the phonons spatially. This introduces an uncertainty on **q**, the reduced wave vector in the Brillouin zone, (the selection rule is broken by crystalline imperfection) and, because dispersion curves are not symmetrical with respect to CBZ, the "sampling" of **q**-space induces band shifting and asymmetry. To a first approximation, Raman line broadening can be described by the (linear) dependence of its half-width upon the inverse grain size, as reported previously for many nanocrystalline materials including CeO_2, Si, Ge, GaAs and diamond (see References 4 and 5 and references therein).

Peak-fitting procedure

The flowchart of Figure 3 summarises the data analysis procedure. Step-by-step recorded Raman spectra were fitted using appropriate software.[13] No manual pre-treatment such as a baseline correction was applied to the spectra before applying the procedure. When necessary, complex backgrounds were introduced as Gaussians into the data. An example is given in Figure 2 with the decomposition of SiC TO and LO Raman peaks using the spatial correlation model. A spectrum representative

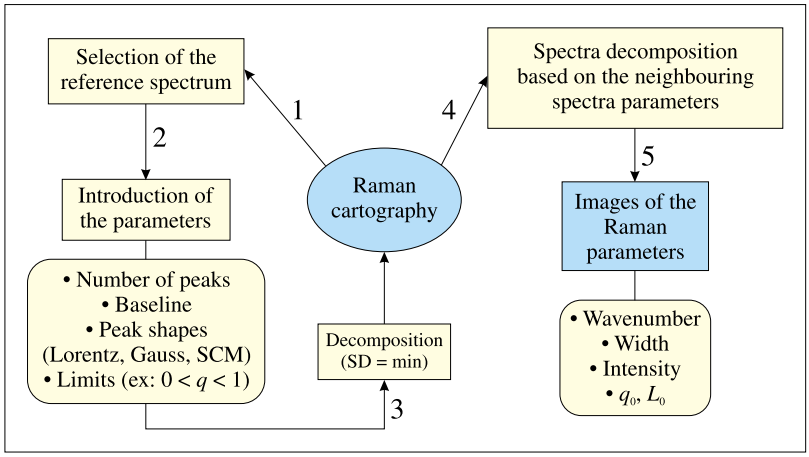

Figure 3. Flow chart of the main steps involved in the building of Raman/Rayleigh "smart" images.

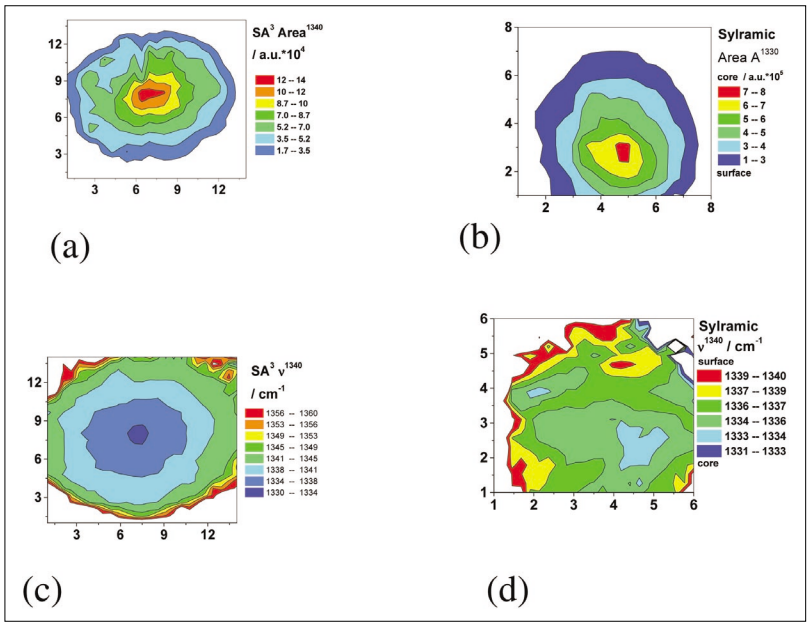

Figure 4. Raman images of SA3® Ube Industry (left) and Sylramic® Dow Corning (right) fibres for D band ($sp^{3/2}$) based on (top) area and (bottom) wavenumber position. (Maps comprise 25 × 25 spectra, 120 s per spectrum; laser excitation wavelength = 632 nm, power = 0.5 mW).[6]

of the whole cartogram (map) is decomposed first. Knowing its position in the Raman map, the resulting data are applied to the neighbouring spectra, so that the standard deviation is minimum to start the decomposition. Then, each spectrum is fitted starting from the data coming from its neighbour. The calculation is short (a few seconds per spectrum) when the model contains only Gaussians and/or Lorentzians. However, each dissymmetrical peak (see Figure 2) introduced into the model increases the calculation time by a factor of five or more. A typical decomposition with 10 symmetrical and three dissymmetrical peaks takes about one minute per spectrum with a 1.8 GHz processor. The image of the parameters is finally presented using commercially-available software.

Raman images

Figure 4 illustrates how Raman microspectrometry can be used to study nanophase distribution in SiC fibres. In order to point out the most important aging factors, we selected fibres for aerospace applications, prepared by different technologies. The Tyranno SA3® fibre (UBE Industry, Japan) is synthesised from graft PCS (polycarbosilane) where organic groups containing aluminium as a crystal growth inhibitor replace methyl groups. Reticulation is obtained by 160°C thermal oxidation, the resulting oxicarbide being carbothermally reduced at 1400°C under inert

gas, before decomposition at 1800°C (with CO release). It has been claimed that the glassy silica layer of the SA3® fibre has a remarkable alkali resistance.[14] The Sylramic® fibre (Dow Corning, USA) is also synthesised from graft PCS but methyl groups are replaced by organic groups containing boron and titanium. The fibre is made out of 96% wt β-SiC nanocrystals.[15] The aluminium contained in SA3® fibres leads to a better creep resistance than the TiB_2, which precipitates in the Sylramic®.

The Raman peak position indicates the chemical nature of the analysed phase, the area is related to its concentration and the precise wavenumber shift gives information on both the nature of the species (especially for resonant lines like the D band at *ca.* 1330 cm^{-1}) and the strain level.[4] The band-width is related to the short-range order of the phase. Colomban *et al.*[7,16,17] have discussed the assignment of Raman peaks in disordered carbons. High crystallinity diamond and graphite have sharp peaks at 1331 and 1581 cm^{-1}, respectively. The two main bands of amorphous carbons are then assigned to diamond-like (D band) and graphite-like (G band) entities. Because the Raman scattering cross-section of diamond is much lower than that of graphite (~10^{-2}), a weak C_{sp^3}–C_{sp^3} stretching mode is expected. In fact, given the small size of carbon moieties, the contribution of the chemical bonds located near their surface will be large. The D band can then be assigned to vibrations involving C_{sp^3}-mixed $C_{sp^2}/_{sp^3}$ bonds here after called $sp^{2/3}$. This band has a strong resonant character (contrary to sp^3 C mode in diamond), as seen by a high dependence of the intensity and position on wavenumber.[7]

Raman images of SA3® and Sylramic® fibres cross-sections (Figure 4) indicate that the core and skin carbon species have a different nature and concentration. The fibre's core is carbon-rich and, in the case of SA3® fibre, the D band is up-shifted by ~30 cm^{-1} from the core to the surface (indicating "aromatisation"). This shift is significant and due to a transformation of the C–C bond. The SA3® is a "carbon-rich tube", while in Sylramic® the carbon rate increases gradually from the surface to the core. This difference between the two fibres can be linked to the manufacturing process. During the spinning phase, the viscosity difference between long and short polycarbosilane chains leads to concentration gradients. Smallest chains having a lower viscosity could preferentially migrate to the fibre's core. Since they are highly concentrated in carbon, due to the high concentration in polymer chain end groups, they induce carbonated species concentration gradients. We will show that these heterogeneities have important consequences on the fibre mechanics.

Material properties and characteristics from Raman parameters

The relationship between grain size and materials' properties is known for a large number of materials. Once the relationship between Raman parameters and grain size is established, it become possible to correlate the Raman parameters with material properties. We can even use Raman measurements to predict the properties present in the different parts of a material. For example, for CeO_2, an electrolyte for high temperature fuel cells, and its electrical properties (e.g. the concentration of defects), prediction from Raman data was in agreement with electrochemical and thermodynamical measurements.[5] The prediction of the mechanical properties of SiC fibres from Raman spectra is also possible. A model based on the intensity ratio of the two main carbon Raman peaks (I_D/I_G) has been proposed to calculate the size of short-range ordered vibrational units in carbon moieties.[6,12] This model

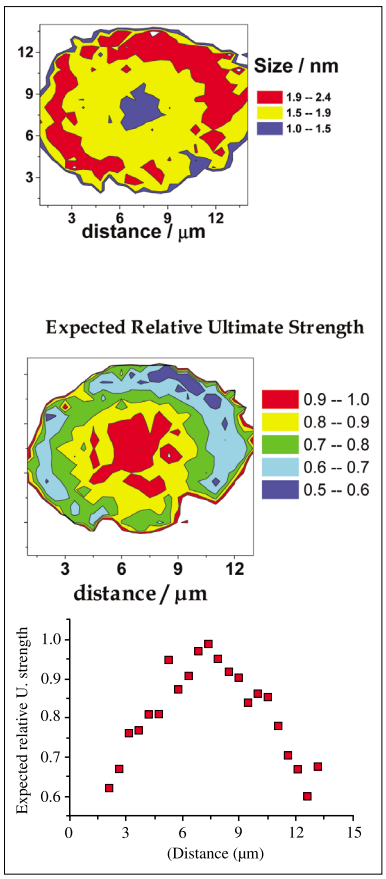

Figure 5. Examples of "smart" images: size distribution of carbon grains in a SiC fibre cross-section, calculated using the correlation between the coherent length and the Raman peaks ratio I_D/I_G.[6] The availability of a relationship correlating Raman studies,[20] TEM examination and the ultimate strength measurements[19] is used to predict the relative mechanical strength in the different fibre regions.

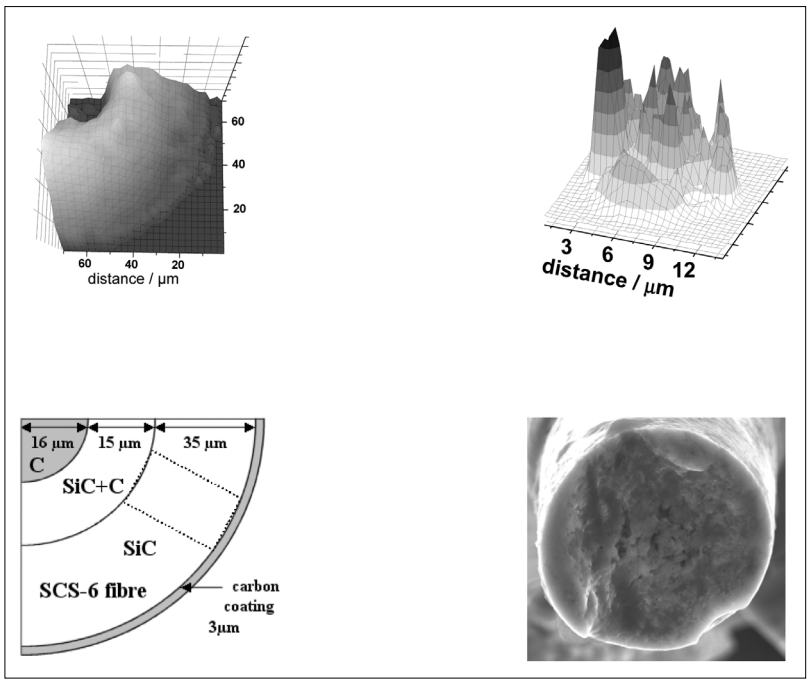

Figure 6. Example of Rayleigh images. Top: left, viewing of the roughness in the mixed SiC + C region of a polished SCS-6 Textron™ fibre used in a metal matrix composite; right roughness of a SA3® Ube Industry SiC fibre used for ceramic matrix composites after alkaline and oxidising corrosion. Bottom: left, schematic of the SCS-6 fibre microstructure; right, SEM micrograph of the SA3 fibre.[6,13]

takes the relative Raman efficiency (noted d) of D^{1350} band (with respect to that of G^{1600}) into account, as well as R, the ratio of surface to core atoms, the surface thickness e_t and, the coherent length (~ the grain size L_g). Assuming a spherical shape of all grains:

$$d \times R \approx d \times \left[\left(1 - \frac{2 \times e_t}{L_g} \right)^{-3} - 1 \right]$$

This model has been used to calculate carbon grain size distribution in the as-received SA3® cross-section (Figure 5). A ring of bigger carbon species appears on the fibre's periphery indicating a higher short-range order, which is consistent with the decrease of the Raman peaks widths. This size increase near the surface can be linked to the elaboration process revealing a higher temperature experienced in this area. Heat-treated fibres show a large increase of this ring. The observed size distribution indicates that crystal growth of the carbon moieties is obtained even deep in the fibre (a small area of low short range order remains at the core). The relationship between Raman parameters and mechanical properties allows one to convert the Raman image to a predictive "mechanical" image. As an example we present in Figure 5 the expected ultimate strength to be achieved for the different fibre regions. In this example the highest values are expected from the fibre core. Other types of fibres exhibit homogeneous behaviour or inverse configuration. Note that if a map gives a didactic view, a line-scan offers a better compromise between rapidity and quality of the information.

Figure 6 shows two examples of the sort of information that may be visualised in images derived from Rayleigh scattering. The Rayleigh images show: (i) a mixed SiC–C region of a "composite" SCS-6™ Textron fibre, and (ii) the Rayleigh image of SA3® Ube Industry SiC fibre cross-section after alkaline and oxidising corrosion, representative of the degradation in a jet engine.[6,18] After corrosion, the SEM image shows the core is rougher than the periphery. The Rayleigh image, which enhances visualisation of the surface roughness, reveals changes in surface topography, which can be analysed quantitatively and correlated with corrosion duration. (However, note that the differentiation between topological and composition information is not always straightforward.)

Improving the quality of Raman and Rayleigh images

The light intensity progressively decreases from the centre to the edge of the laser focus spot. Typically, for the spot obtained with a 100× long focal-length objective, the diameter is approximately 1 µm for green excitation and the "edge region" has a thickness of ~0.5 µm, as determined from a line-scan across a metal–dielectric interface. Taking this effect into account, the sharpness of the image can be restored to that expected from the material geometry. Figure 7 shows the scanning electron microphotograph (SEM) of a SiC fibre reinforced SiC matrix composite prepared by Chemical Vapour Infiltration and subjected to strong alkaline and oxidising corrosion. Specific coatings have been deposited on the fibres to optimise the thermomechanical properties of the material. Figure 7 compares the original

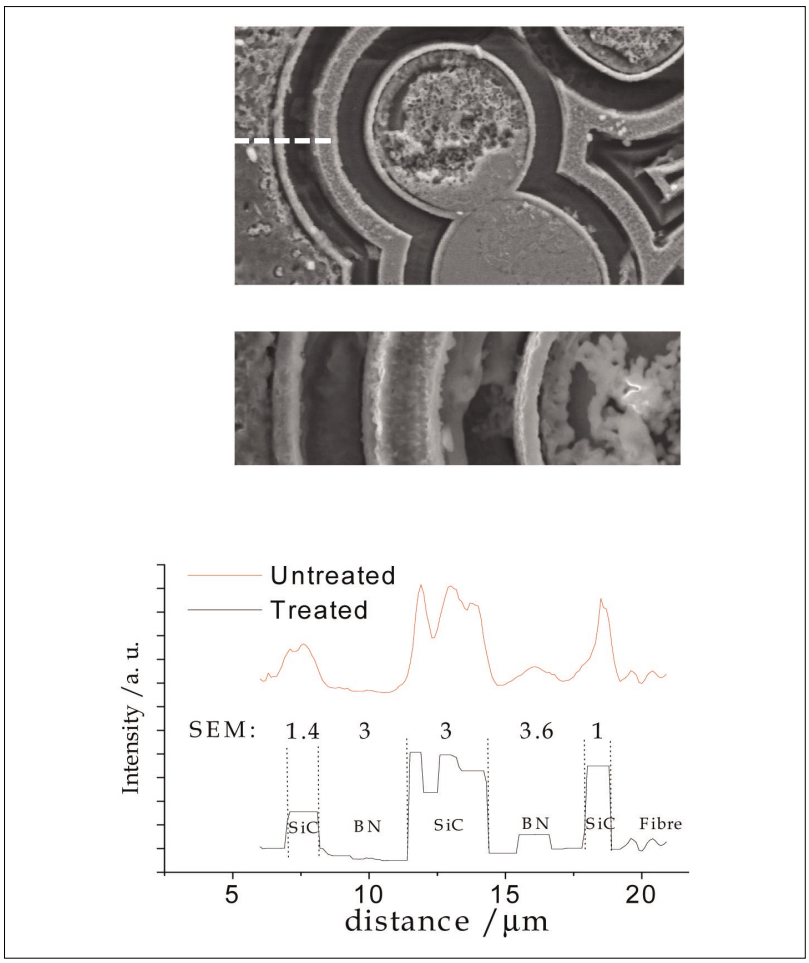

Figure 7. SEM micrograph of a SiC/SiC composite (prepared by CVI) after a strong corrosion. A Rayleigh line-scan has been made along the dashed line. The original Rayleigh line-scan and that obtained after correction for the laser focus spot intensity variation are compared. A good agreement is noted between the thickness measured on the corrected line-scan and the SEM micrograph. The different levels of corrosion of the various fibre coatings are clearly observed. (Laser excitation wavelength = 632 nm; 100x objective, Jobin-Yvon Raman Infinity Instrument, 200 spectra, 0.5 s per spectrum).

Rayleigh line-scan and that obtained after correction for the laser spot size intensity variation. Note the thickness obtained with this corrected scan is in good agreement with that determined from SEM measurements. Similar treatment can be performed on Raman line-scans and images.

Conclusion

Raman and Rayleigh images are well suited for the analysis of nanophased materials and to highlight differences in bulk and skin nanostructure and reactivity. The use of appropriate models to simulate the Raman spectra and to describe their dependency on grain size allows one to build correlations between Raman (and in some cases Rayleigh) spectra and grain size and grain size dependant properties. The developments of procedures for enhancing the spatial resolution offer very promising potential for the further understanding and the optimisation of advanced material properties.

Acknowledgements

The author thanks his former PhD students and post-docs (J. Wu, S. Karlin, G. Gouadec, M. Havel) and collaborators (G. Sagon, D. Baron) for their important contributions in the research presented. Special thanks to Dr G. Gouadec for many fruitful discussions.

References

1. Ph. Colomban, *Ceramics International* **15,** 23–50 (1989).
2. L.C. Klein (Ed.), *Sol-Gel Technology*. Noyes Publications, Park Ridge, New Jersey (1988).
3. (a) S. Padovani, C. Sada, P. Mazzoldi, B.G. Brunetti, I. Borgia, A. Sgamellotti, A. Giulivi, F. d'Acapito and G. Battaglin, *J. Appl. Phys.* **93**, 10058 (2003); (b) J; Pérez-Arantegui, J. Molera, A. Larrea,T. Pradell, M. Vendrell-Saz, I. Borgia, B.G. Brunetti, F. Cariati, P. Fermo, M. Mellini, A. Sgamellotti and C. Viti, *J. Amer. Ceram. Soc.* **84,** 442 (2001).
4. (a) Ph. Colomban, *Ceram. Eng. & Sci. Proc.* **21(3),** 143–153 (2003); (b) Ph. Colomban, *Ceram. Eng. & Sci. Proc.* **24(4),** in press (2003).
5. (a) I. Kosacki, V. Petrovski, H. Anderson and Ph. Colomban, *J. Amer. Ceram. Soc.* **85(11),** 2646–2650 (2002); (b) I. Kosacki, T. Suzuki, H. Anderson and Ph. Colomban, *Solids State Ionics* **149,** 99–105 (2002).
6. M. Havel and Ph. Colomban, *J. Raman Spectrosc.* **34(10),** 786–794 (2003).
7. G. Gouadec, Ph. Colomban and N.P. Bansal, *J. Amer. Ceram. Soc.* **84(5),** 1129–1135 (2001).
8. D.W. Feldman, J.H. Parker, W.J. Choyke and L. Patrick, *Phys. Rev.* **173(3),** 787–793 (1968).
9. A. Surca-Vuk, B. Orel, G. Drazic and Ph. Colomban, in *Nanostructured Materials*, Ed by H. Hofman, Z. Rahman and U. Schubert. Springer Verlag, Wien, pp. 153–172 (2002).
10. E. Duval, *Phys. Rev.* **B49,** 5795–5799 (1992).
11. P. Parayanthal and F.H. Pollak, *Phys. Rev. Lett.* **52(20),** 1822–1825 (1984).
12. S.A. Solin and N. Caswell, *J. Raman Spectrosc.* **10,** 129 (1981).
13. M. Havel, D. Baron and Ph. Colomban, *J. Mater. Sci.*, submitted.
14. T. Ishikawa, Y. Kohtoku, K. Kumagawa, T. Yamamura and T. Nagasawa, *Nature* **391,** [6669] 773–775 (1998).
15. J. Lipowitz, J.A. Rabe, K.T. Nguyen, L.D. Orr and R.R. Androl, *Ceram. Eng. & Sci. Proc.* **16,** 55–64 (1995).
16. S. Karlin and Ph. Colomban, *Composites, Part B* **29B,** 41–50 (1998).
17. Ph. Colomban, *J. Korean Ceramic Society* **5(1),** 55–72 (1999).
18. M. Havel and Ph. Colomban, *Composite Part B: Engineering* **35(1),** in press (2004).
19. M.-H. Berger, N. Hochet and A.R. Bunsell, *Ceram. Eng. & Sci. Proc.* **19,** 39–46 (1998).
20. G. Gouadec and Ph. Colomban, *J. European Ceramic Soc.* **21(9),** 1249–1259 (2001.)